Paper CFDSC-2013 #186, Session 11–2 - Unsteady Aerodynamics,
21th Annual Conference of the CFD Society of Canada,
Sherbrooke, Canada, May 6–9, 2013.

RANS versus Scale-Adaptive Turbulence Modeling for Engineering Prediction of Oscillating-Foils Turbines

Etienne Gauthier, Thomas Kinsey and Guy Dumas

Laboratoire de Mécanique des Fluides Numérique, Département de Génie Mécanique,
Université Laval, Québec, G1V 0A6, Canada

Email: *etienne.gauthier.4@ulaval.ca*

ABSTRACT

This study aims to compare the performance predictions of an oscillating foil in power-extraction regime using two different turbulence modeling approaches: an Unsteady Reynolds-Averaged Navier-Stokes approach (URANS) using the Spalart-Allmaras model and a hybrid approach using the Scale-Adaptive Simulation model (SAS). The main goal is to evaluate the influence of a finer capture of the wake turbulent structures on a single oscillating hydrofoil performances. Simulations in 2D and 3D are considered. This work is part of a broader investigation on the impact of multi-bodies interactions on the hydrokinetic turbine performances. Two cases presenting different levels of turbulent structures generation have been used. For the smooth case, performance parameters and physical fields closely match between the S-A model and the SAS model. The second case characterized by the occurance of important leading edge vortex shedding (LEVS) presents notable differences between predictions of the instantaneous forces and moment coefficients from both models. However, mean performance diagnostics are found to be little affected. Significant differences are furthermore observed in the wake structure using the SAS turbulence model compared to the S-A turbulence model which should prove to be a definitive advantage when considering multi-bodies interactions.

1 INTRODUCTION

With the growing demand in energy and the depletion of fossil fuels, the renewable energy sector plays a key role in the international strategy for a sustainable development. After a rapid growth of the wind energy sector in the last few decades, other promising alternative energy sources are emerging. From these, hydrokinetic turbines present an interesting potential. This type of device is used to convert the kinetic energy from rivers and tidal flows into electricity.

As in the wind turbine sector, the development of hydrokinetic turbines mainly focuses on horizontal-axis rotor blade devices. However, another innovative way of extracting energy from flows using oscillating wings was analytically and experimentally investigated by McKinney and DeLaurier [1] in 1981. Further experimental and numerical investigations have been achieved by Jones et al. [2] in 2003.

A concept of a power extracting device based on oscillating hydrofoils (referred to as HAO: Hydrolienne à Ailes Oscillantes) has been under development for several years at the Laboratoire de Mécanique des Fluides Numérique (LMFN) of Laval University [3-7].The power-extraction potential of this technology has been successfully demonstrated through CFD simulations [3-5-6-7] and experiments [4] in recent years. Comparing results from 3D URANS simulations with field measurements, Kinsey and Dumas [5] observed an excellent agreement on power-extraction efficiency in the case of a single oscillating foil. However, in the case of two foils oscillating in a tandem configuration, the predicted efficiency from URANS simulations tend to overpredict the power extracted for reduced frequencies over 0.1. One hypothesis advanced for this behavior is an over-diffusion of the wake shed by the upstream foil due to the URANS modeling. Effects on instantaneous forces would be small in the case of the upstream foil, but potentially important for the downstream foil which is oscillating in the wake of the upstream foil. There is thus a need to explore other types of turbulence modeling. In addition to multiple-foils interactions, further development and improvement of the HAO design in realistic flow conditions require to take into account the interaction with the mounting structure of the turbine.

The present ongoing study investigates the impact of different levels of turbulence modeling on the performance predictions of a single hydrofoil in 2D and 3D with finite span. The procedure consists of carrying out simulations for two different cases presenting distinct near-wake characteristics. The first case considered presents smooth trailing edge shedding (case 1), the second case presents important LEVS at top and bottom heaving position (case 2). This investigation thus addresses the impact of a finer capture of turbulent structures in two typical scenarios of application. It is a necessary step towards the development of a general and robust methodology to simulate reliably the entire hydrokinetic turbine.

2 PROBLEM DESCRIPTION

The present work considers a single hydrofoil NACA0025 at a Reynolds number ($Re = U_\infty c/\nu$) of 500 000 undergoing a combined heaving $h(t)$ and pitching $\theta(t)$ motion in a uniform flow as sketched on Fig. 1. The position of the hydrofoil is defined as

$$\theta(t) = \theta_0 \sin(\gamma t) \tag{1}$$

$$h(t) = H_0 \sin(\gamma t + \phi) \tag{2}$$

and the corresponding velocities,

$$\Omega(t) = \theta_0 \gamma \cos(\gamma t) \tag{3}$$

$$V_y(t) = H_0 \gamma \cos(\gamma t + \phi) \tag{4}$$

where θ_0 and H_0 are respectively the pitching and heaving amplitude, Ω is the pitching velocity, V_y is the heaving velocity, γ is the angular frequency ($2\pi f$) and ϕ is the phase difference between the two motions. In this study, the pitching axis is located on the chord line at a distance $x_p/c = 0.4$ from the leading edge. The pitching amplitude is $\theta_0 = 70°$, the heaving amplitude is $H_0/c = 1$ and ϕ is kept constant at 90°. The reduced frequency is defined as $f^* = fc/U_\infty$. The only parameter that differs between the smooth case (Case 1) and the case with LEVS (Case 2) is the reduced frequency. The case 1 involves a reduced frequency of 0.18 while the case 2 operates at a reduced frequency of 0.08.

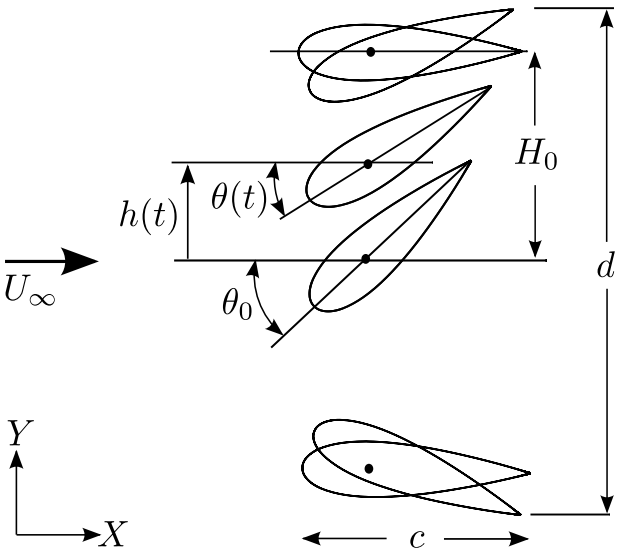

Figure 1: *Imposed heaving $h(t)$ and pitching $\theta(t)$ motions.*

Forces, moment and power coefficients are used to analyze the performances and are defined as

$$C_X = \frac{X}{\frac{1}{2}\rho U_\infty^2 b c} \tag{5}$$

$$C_Y = \frac{Y}{\frac{1}{2}\rho U_\infty^2 b c} \tag{6}$$

$$C_M = \frac{M}{\frac{1}{2}\rho U_\infty^2 b c^2} \tag{7}$$

$$C_P = \frac{P}{\frac{1}{2}\rho U_\infty^3 b c} \tag{8}$$

where X and Y are respectively the horizontal and vertical hydrodynamic forces, M is the torque at the pitching axis, P is the power extracted by the hydrofoil (rate of work done by the flow on the foil) and b is the foil span. The total power extracted is the result of both contributions associated to the heaving motion $P_y(t)$ and to the pitching motion $P_\theta(t)$ and computed as

$$P_y(t) = Y(t) V_y(t) \tag{9}$$

$$P_\theta(t) = M(t)\,\Omega(t). \tag{10}$$

To evaluate the efficiency of the oscillating hydrofoil, the mean power extracted has to be compared to the upstream power available P_a through the frontal flow area

$$\eta \equiv \frac{\overline{P}}{P_a} = \frac{\overline{P}_y + \overline{P}_\theta}{\frac{1}{2}\rho U_\infty^3 b d} \tag{11}$$

where d is the overall vertical extent of the foil motion as seen in Fig. 1, which in this case is $d = 2.4238c$. The efficiency is limited to a maximum theoretical value of 59% from the Betz limit which is derived from the analysis of an inviscid stationary stream tube [8].

3 NUMERICS

The finite volume code ANSYS Fluent 14.5 [9] is used in this work with a double precision solver. A Semi-Implicit Method for Pressure Linked Equations algorithm (SIMPLE) is used for the velocity-pressure coupling. Second-order schemes are used for pressure, momentum and turbulent quantities discretizations. The unsteady formulation is based on a second-order implicit scheme. When the SAS model is used, the momentum equations are discretized with a bounded central discretization while the unsteady formulation is based on a bounded second-order implicit scheme. For the 2D cases, seven cycles of motion were computed to obtain converged statistics, i.e., a variation of the efficiency η from one cycle to the other of less than 0.1%. For the 3D cases, only two

Mesh	Total cells	Nodes on foil section	Nodes on foil span	AR
2D-1	50 000	380	-	-
2D-2	170 000	760	-	-
3D	7 910 000	380	90	10

Table 1: *Meshes characteristics.*

transitory cycles were performed after an impulsive start. A third cycle was then carried out for the purpose of diagnostics and a relative difference of less than 0.3% was obtained between the second and the third cycle.

In the present numerical methodology, the heaving and pitching motions are defined separately. The simulation are performed in a reference frame heaving with the foil. This requires to specify time-varying boundary conditions on the top, bottom and inlet boundaries as well as the acceleration of the heaving reference frame as a source term in the Navier-Stokes equations. These are prescribed to the solver through User-Defined Functions (UDF). The use of a circular non-conformal sliding mesh interface allows the foil to pitch in the heaving reference frame.

The boundary conditions and the dimensions of the domain for the 3D configuration are presented in Fig. 2. The symmetry condition allows the simulation of only a half-span hydrofoil. For all the simulations, the turbulence settings at the inlets are a turbulence intensity of 0.1% and a turbulence viscosity ratio of 0.01, i.e., a clean upstream flow.

The main characteristics of the meshes used in this study are presented in Table 1. The motion definition requires two different mesh zones bounded by a non-conformal sliding mesh interface as shown in Fig. 3. The refined zone downstream the hydrofoil ensures a better capture of the wake structures. As described in Fig. 4, the mesh is refined towards the wingtip.

3.1 Turbulence modeling

The Spalart-Allmaras model (S-A) was found to give good predictions of the hydrokinetic turbine performances compared to experimental data in previous works especially in the case of a single oscillating foil [5]. Further optimization of this turbine technology requires the evaluation of the impacts of multi-bodies interactions on the device performances. Thus, turbulence modeling is a critical aspect to study. In this ongoing work, URANS methods are compared with higher-level turbulence modeling approaches. Although LES (large eddy simulation) methods would circumvent the known weaknesses of RANS models when dealing with some flow separation phenomena, their prohibitive computing cost leads us to a compromise. Among the alternative approaches, hybrid methods such as DES (detached eddy simulation) and Scale-Adaptive Simulation (SAS) are attractive. The present work focusses on the SAS model.

The Scale-Adaptive Simulation method can be defined as a second generation URANS method rather than a sub-grid scale modeling approach because the model does not contain any parameter related to the grid used for the resolution of the

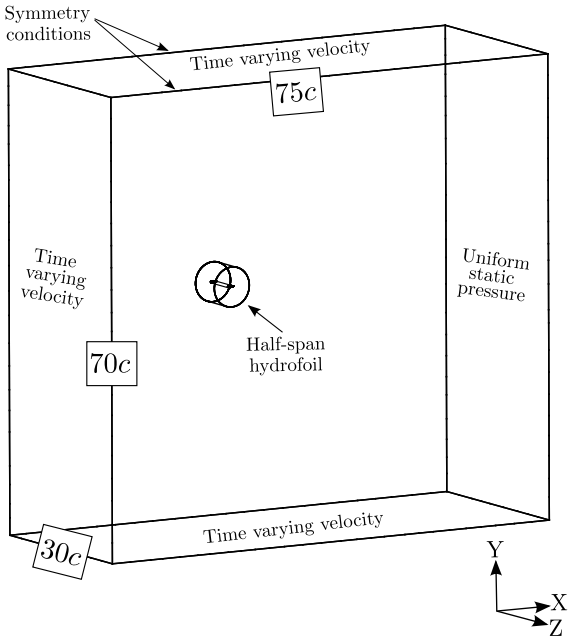

Figure 2: *3D domain and boundary conditions.*

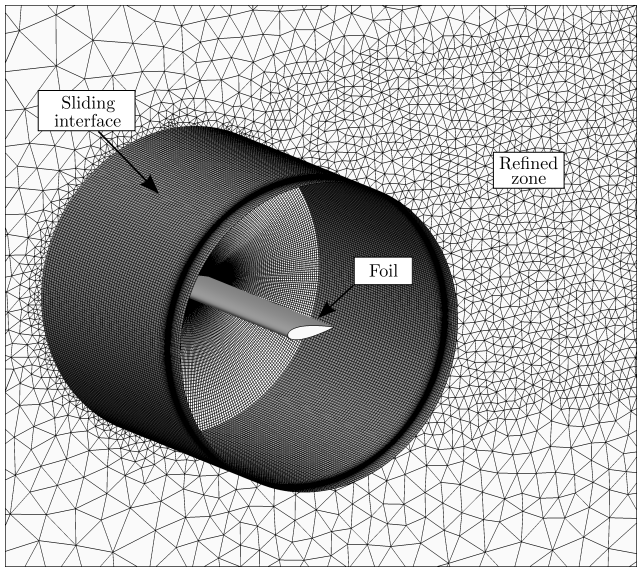

Figure 3: *3D mesh details: non-conformal interface and refined zone downstream of the foil circular zone.*

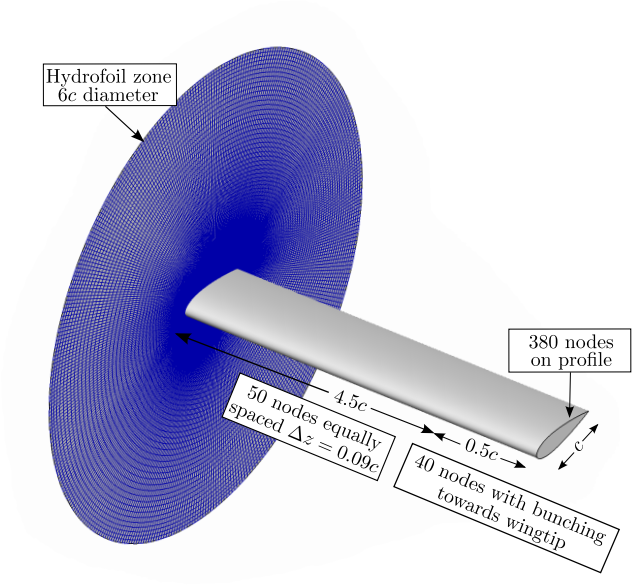

Figure 4: *Spanwise discretization.*

transport equations (which would be the case for LES or DES modeling) [10]. This model was developed by Menter & al. [11] by revisiting the $k-kL$ model developed by Rotta. In the modifications made to the Rotta model, a second length scale is introduced in the transport equations, the von Kàrmàn length-scale L_{vk}. The addition of this second length-scale allows the model to exhibit both steady solutions as well as scale-resolving characteristics depending on the flow situation. The model provides RANS resolution in stable flow regions and allows the resolution of some of the turbulent spectrum in unstable flow regions.

The main difference between standard URANS resolution and Scale-Adaptive methods is in the treatment of resolved turbulence. In URANS methods, the resolved scales are damped relatively quickly and the simulations tend to produce only large-scale unsteadiness. In contrast, the SAS method allows the formation of a fuller (but still incomplete) turbulent spectrum by adjusting its length-scale to the resolved structures leading to a better definition of the latters. The transition from RANS to SAS resolution is triggered by the level of flow instabilities. If the instabilities are too weak, the model does not switch to a SAS resolution and remains a URANS resolution. This implies that SAS methods are most promising in flows with significant instability mechanisms present such as in the near wake of bluff bodies [10].

3.2 Time and space refinements

To assess the independence of results with respect to time and space discretizations, simulations were performed with two levels of time refinements as well as two levels of space refinements. Results of these simulations are provided in Table 2 and 3. We find that to increase the number of time steps per cycle from 2000 to 4000 has essentially no effect on monitored forces with relative differences within 0.15% for all quantities. Therefore, a time discretization of 2000 time steps per cycle is deemed sufficiant. As for the space discretization, mesh 2D-1 and 2D-2 described in Table 1 are used. For case 1, cycle-averaged and peak values of forces and moment coefficients closely match within 0.8% between both meshes. For the case that presents important LEVS, differences between mesh 2D-1 and mesh 2D-2 are quite small on the cycle-averaged values of C_X and the peak values of C_Y, as the relative difference remains less than 1.3%. However, results show significant sensitivity on the instantaneous moment coefficient peak values. Despite these differences

	Mesh	ts/cycle	$\overline{C}_X$	$\hat{C}_Y$	$\hat{C}_M$	η, %
S-A						
Time	2D-1	2 000	1.334	2.324	0.681	35.62
	2D-1	4 000	1.332	2.323	0.681	35.61
Space	2D-1	2 000	1.334	2.324	0.681	35.62
	2D-2	2 000	1.323	2.310	0.683	35.40
SAS						
Time	2D-1	2 000	1.297	2.279	0.685	34.70
	2D-1	4 000	1.296	2.278	0.685	34.70
Space	2D-1	2 000	1.297	2.279	0.685	34.70
	2D-2	2 000	1.291	2.269	0.685	34.61

Table 2: *Space and time refinements for Case 1 ($f^* = 0.18$), cycle-averaged values of C_X and peak values of C_Y and C_M are provided as well as the efficiency* η.

	Mesh	ts/cycle	$\overline{C}_X$	$\hat{C}_Y$	$\hat{C}_M$	η, %
S-A						
Time	2D-1	2 000	1.696	2.756	0.464	30.22
	2D-1	4 000	1.696	2.756	0.464	30.19
Space	2D-1	2 000	1.696	2.756	0.464	30.22
	2D-2	2 000	1.682	2.751	0.613	29.74
SAS						
Time	2D-1	2 000	1.724	2.739	0.736	29.55
	2D-1	4 000	1.725	2.748	0.735	29.57
Space	2D-1	2 000	1.724	2.739	0.736	29.55
	2D-2	2 000	1.713	2.702	0.794	29.26

Table 3: *Space and time refinements for Case 2 ($f^* = 0.08$), cycle-averaged values of C_X and peak values of C_Y and C_M are provided as well as the efficiency* η.

on instantaneous peak values, a good agreement for cycle-averaged efficiencies within 1.6% is observed.

For 3D simulations, a time discretization of 2000 time steps per cycle and a foil zone based on 2D-1 mesh are used. Future work will provide a rigourous 3D space refinements study.

4 RESULTS

To evaluate the influence of each turbulence modeling approach for an oscillating hydrofoil, two application cases are used. For both cases, the basic configuration parameters are: NACA 0025, $Re = 500\,000$, $H_0/c = 1$, $\phi = 90°$, $x_p/c = 0.4$ and $\theta_0 = 70°$. These parameters are kept constant while the reduced frequency (f^*) is 0.18 for Case 1 and 0.08 for Case 2.

4.1 Influence of turbulence modeling

Vorticity fields at two instants in the oscillation cycle along with instantaneous forces and moment coefficients are provided for Case 1 and Case 2 respectively in Fig. 5 and Fig. 6. For Case 1, the boundary layers remain essentially attached to the foil on the complete cycle. For that smooth case, vorticity fields and time evolution of forces and moment coefficients are similar for both the S-A and the SAS models. For the second case, the lower reduced frequency changes the hydrofoil dynamics and induces LEVS at top and bottom heaving positions as shown in Fig. 6. Turbulence modeling has a greater impact in this case because of the generation of important turbulent structures. Between the S-A and the SAS models, differences are observed on the vorticity fields and on the instantaneous forces and moment coefficients. One notes particularly significant differences in the vortex dynamic at the top heaving position ($t/T = 0$). Also, at quarter period ($t/T = 0.25$), the SAS simulation provides more details in the wake past the trailing edge compared to the smooth wake of the S-A simulation. For both cases, a relative drop of less than 2.6% is observed on the efficiency with the SAS model compared to the S-A model as shown in Table 4. These 2D simulations are mainly used as preliminary results to 3D simulations, for which the SAS model is more targeted.

The 3D analysis is here limited to the case involving generation of important LEVS, therefore for our Case 2. One can observe in Fig. 7 that the simulation using scale-adaptive turbulence modeling presents a generation of finer turbulent structures compared to the averaged structures present with the S-A turbulence model. The lower level of turbulent viscosity ratio obtained with the SAS model compared to the S-A model is attributed to the addition of the second length-scale L_{vK} that adjusts itself to the smallest length-scale of the local turbulence resolved. The general flow pattern is quite similar in both cases, but the break-up of large unsteady structures into smaller vortices with the SAS model seems to spread over a larger spanwise region of the foil compared to a more localized affected region in the simulation using the S-A model. This can also be observed on the pressure contours. On the upper surface of the hydrofoil, at approximately one chord of the wing tip, a suction zone is present with both turbulence models where the main vortex is generated. The breaking of the flow structures with the SAS turbulence model results in a more perturbed field over the foil. This instant in the hydrofoil cycle is interesting for the visualization of turbulent structures but has not a critical impact on performances since the foil is essentially extracting no power at this particular time. This can be observed from the time evolution of the power coefficient (Fig. 9).

The same analysis is made at the quarter period where the power extracted is maximal (Fig. 8). At this time in the cycle, the boundary layers on both foil surfaces are attached. Both turbulence models yield similar pressure fields over the foil. For this case, turbulence modeling changes the spanwise vortical organization in the near wake but the effects on the hydrofoil are limited. Since most power is extracted at this time, global power extraction efficiencies are quite comparable with both approaches.

Indeed, Table 4 presents the 2D and 3D simulation results in term of cycle-averaged performance parameters on the second cycle of calculation for both turbulence models, while Fig. 9 presents the cycle evolution of instantanious forces, moment and power coefficients. For Case 1, the relative difference between the predictions of the S-A model and the SAS model is essentially the same in 2D and 3D. In the case with LEVS (Case 2), the relative difference in efficiency predictions between the S-A model and the SAS model is twice as large in 3D as it is for 2D simulations. The main differences observed is on the moment coefficient peak values that present a drop of 8% with the SAS model compared to the S-A model.

One can finally observes in Fig. 9 that the peak values of moment coefficient with the SAS model in 2D has a significant impact on the power coefficient especially at $t/T = 0.45$ and $t/T = 0.95$ in the oscillation cycle. A better match can be observed on the peak values for the 3D simulations comparing the two turbulence models which explain the relatively good match on the efficiency values.

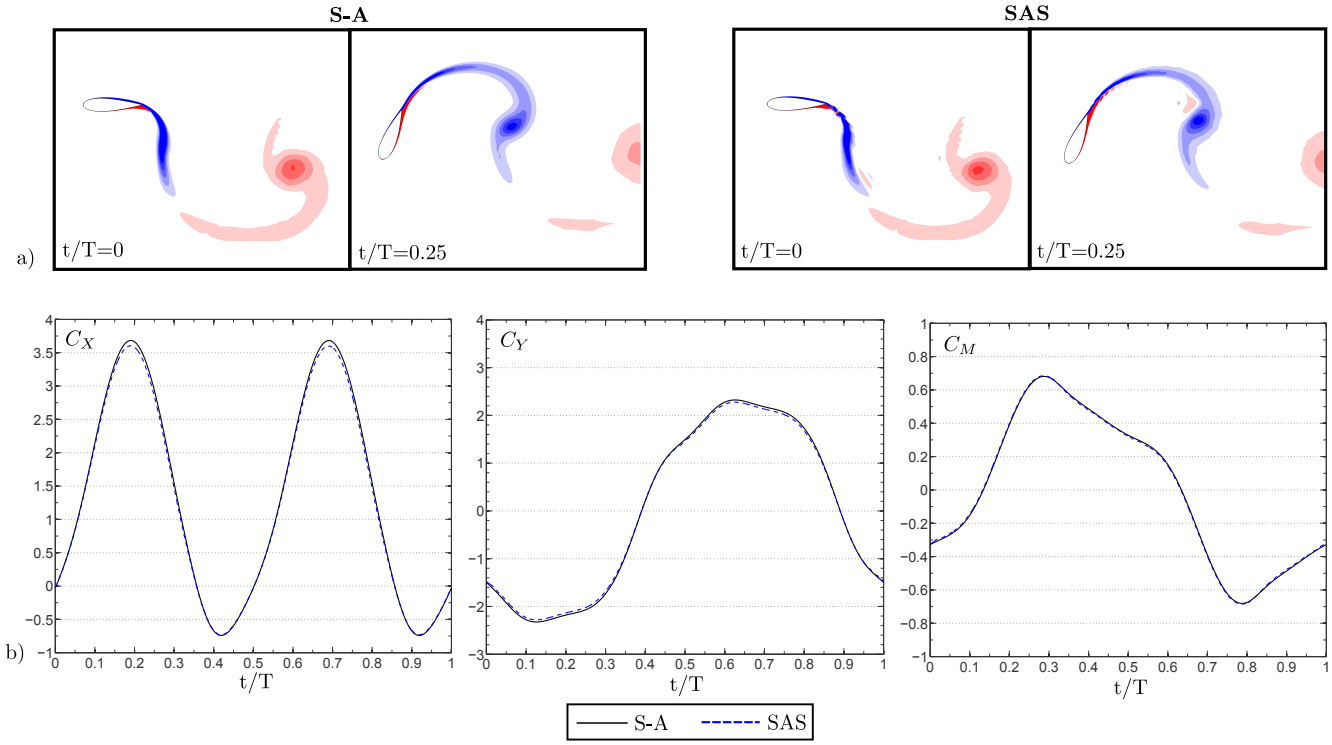

Figure 5: *Overview of the Case 1.* $f^* = 0.18$*: a) Contours of vorticity (red for positive and blue for negative) at two instants in the cycle; b) the time evolution of the force and moment coefficients* C_X, C_Y *and* C_M.

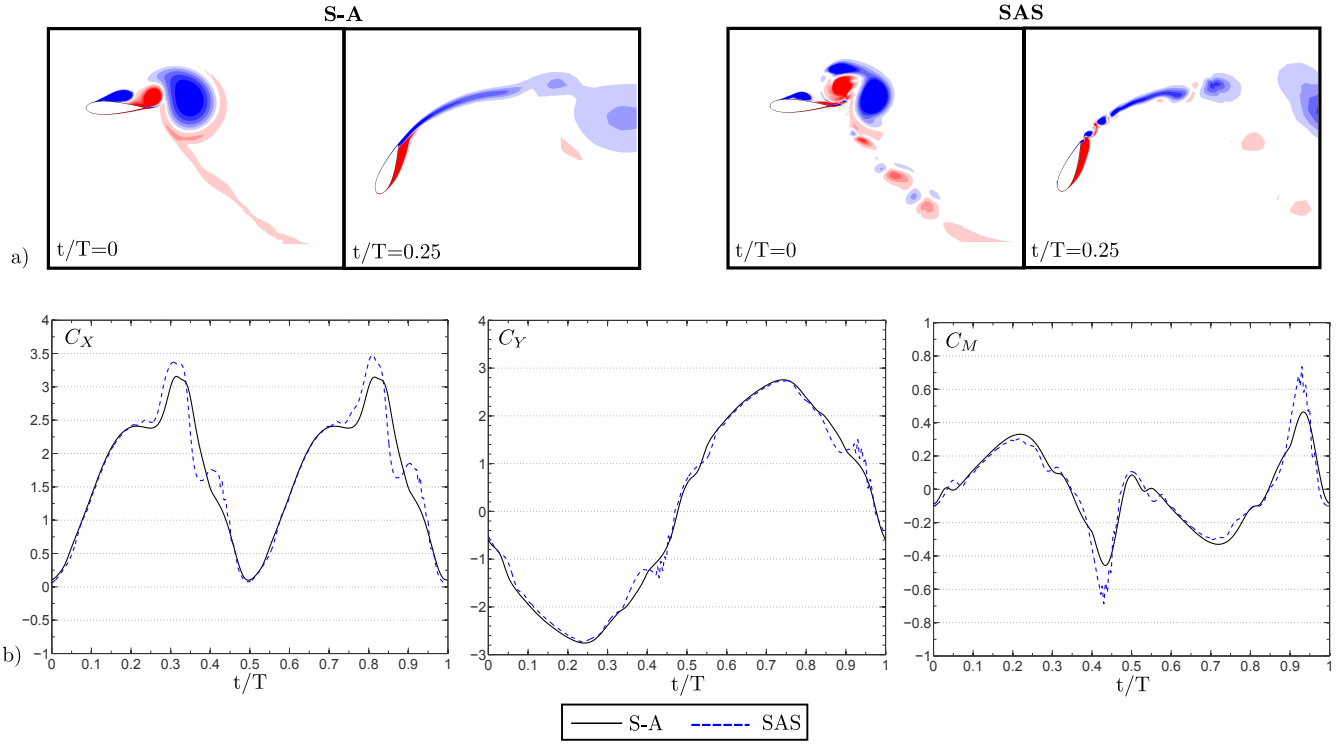

Figure 6: *Overview of the Case 2.* $f^* = 0.08$*: a) Contours of vorticity (red for positive and blue for negative) at two instants in the cycle; b) the time evolution of the force and moment coefficients* C_X, C_Y *and* C_M.

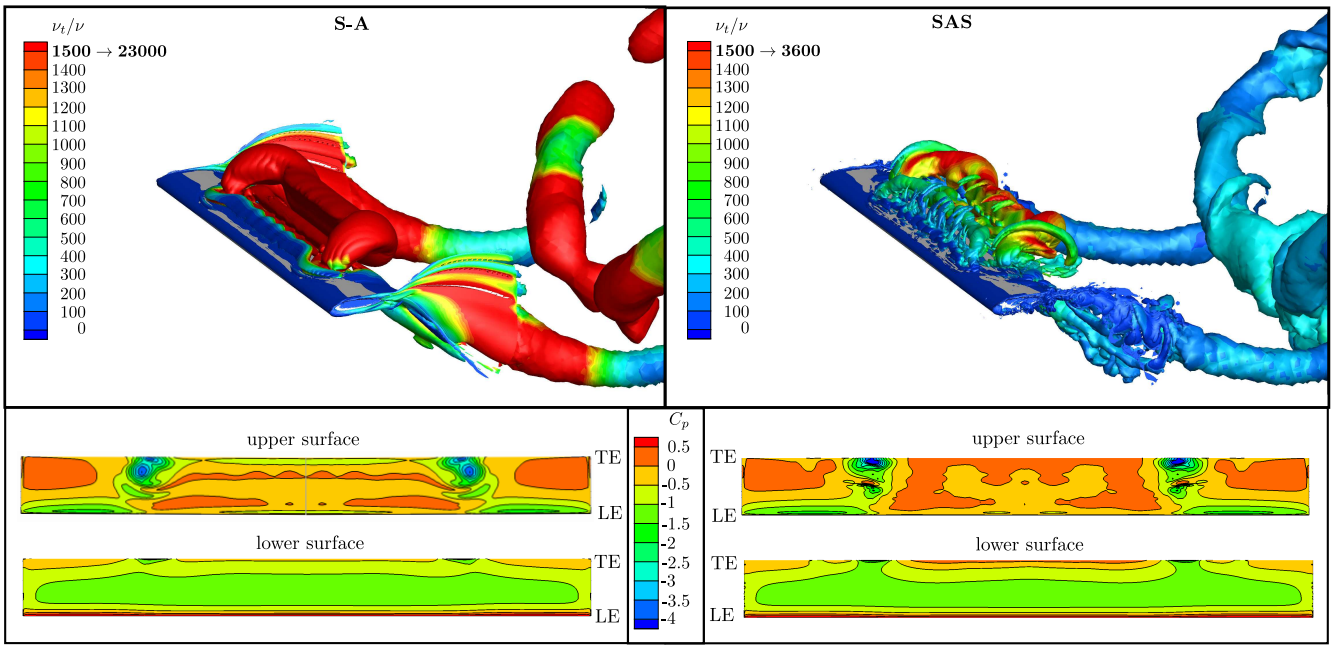

Figure 7: *Turbulence modeling comparison for 3D effects on the hydrofoil at its top position ($t/T = 0$) for Case 2; Flow structure: isosurface of λ_2 vortex criterion ($\lambda_2 = -0.15$) colored by the turbulent viscosity ratio (top) and pressure coefficient contour on the hydrofoil upper and lower surfaces (bottom).*

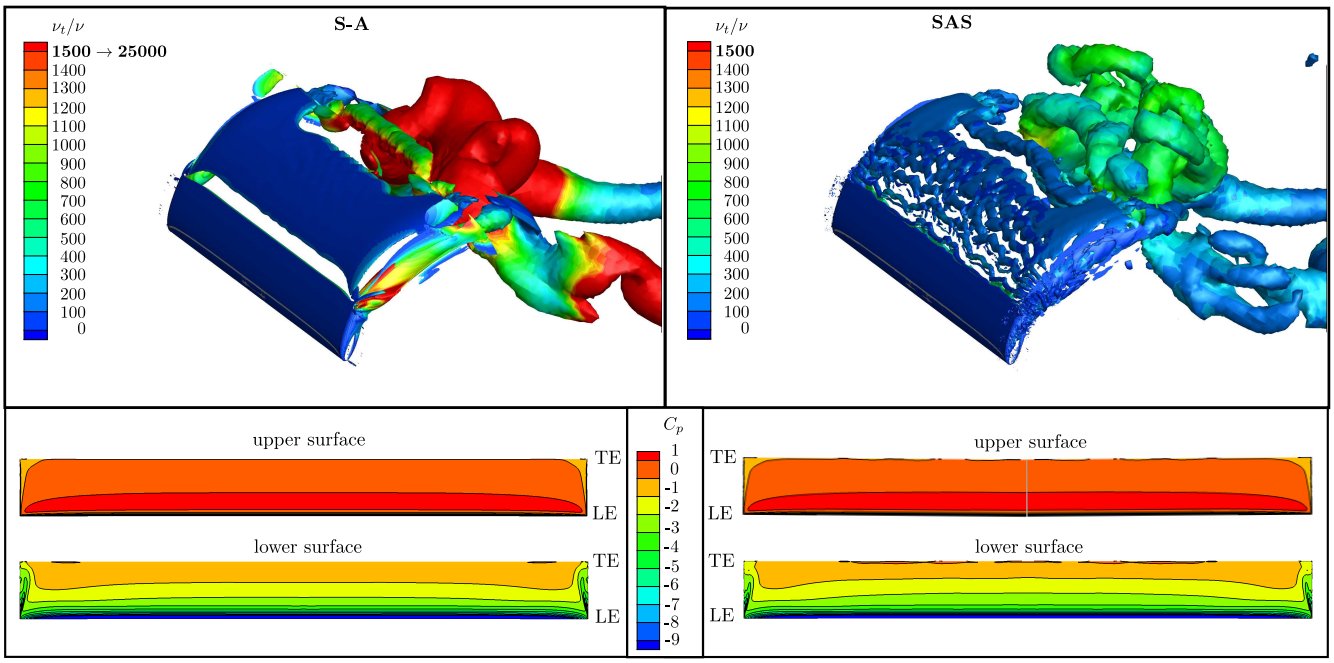

Figure 8: *Turbulence modeling comparison for 3D effects on the hydrofoil at quarter period ($t/T = 0.25$) for Case 2; Flow structure: isosurface of λ_2 vortex criterion ($\lambda_2 = -0.15$) colored by the turbulent viscosity ratio (top) and pressure coefficient contour on the hydrofoil upper and lower surfaces (bottom).*

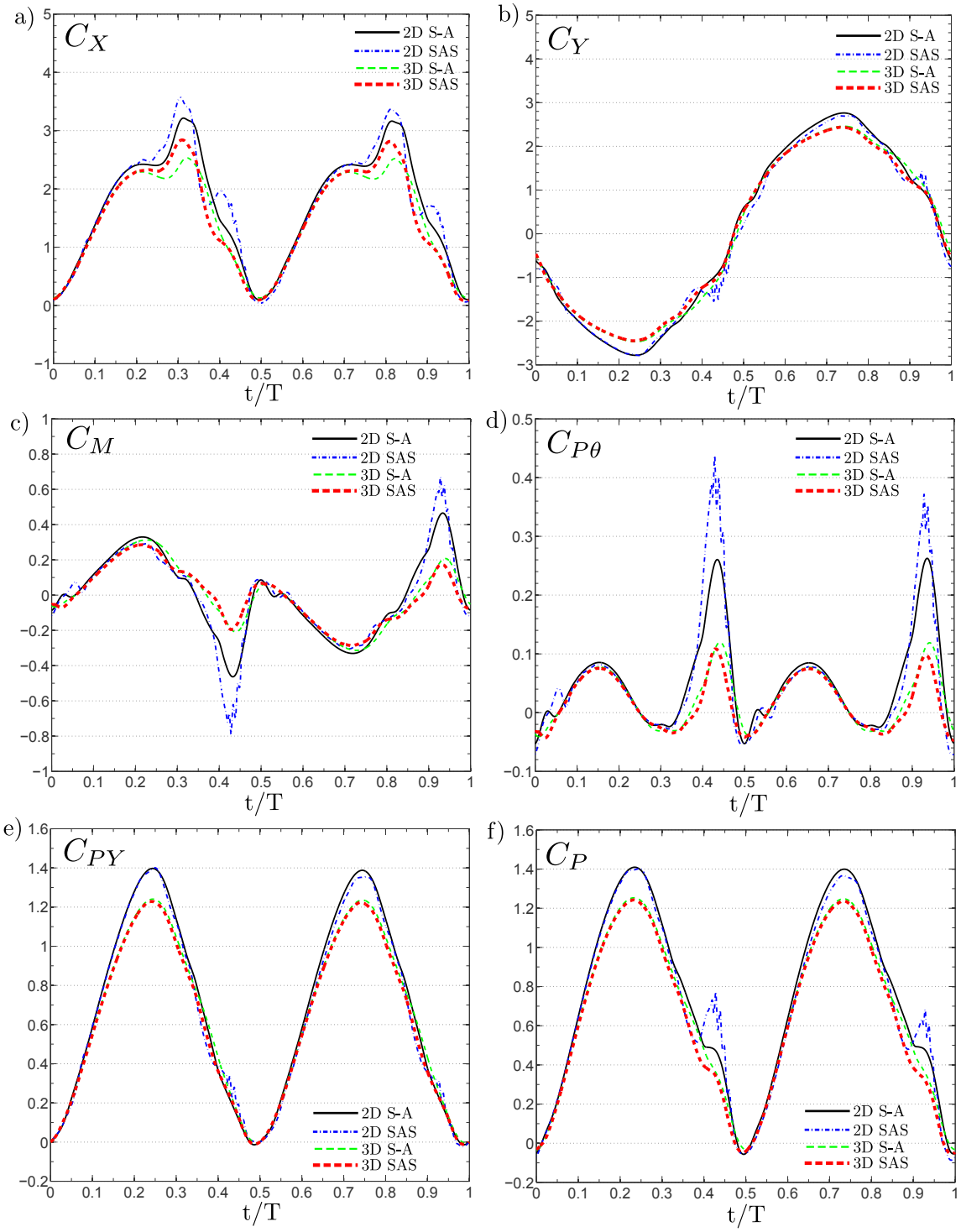

Figure 9: *Comparison of instantaneous forces, moment and power coefficients between 2D and 3D simulations for S-A and SAS turbulence models for Case 2.*

Case	Turbulence modeling	$\overline{C}_x$	$\hat{C}_y$	$\hat{C}_m$	η [%]	$\Delta\eta$ Relative to S-A [%]
Case 1						
2D	S-A	1.351	2.334	0.690	36.40	-
2D	SAS	1.313	2.286	0.693	35.45	-2.62
3D	S-A	1.223	2.171	0.630	30.87	-
3D	SAS	1.186	2.126	0.636	30.01	-2.81
Case 2						
2D	S-A	1.706	2.763	0.466	30.34	-
2D	SAS	1.732	2.696	0.670	29.71	-2.07
3D	S-A	1.503	2.460	0.313	27.42	-
3D	SAS	1.511	2.440	0.285	26.31	-4.02

Table 4: *Comparison 2D versus 3D for the second oscillation cycle after the impulsive start, cycle-averaged values of C_X and peak values of C_Y and C_M are provided as well as the efficiency η.*

5 CONCLUSION

In this paper, Spalart-Allmaras and Scale-Adaptive turbulence model have been employed to simulate the flow over a single hydrofoil oscillating in a free stream flow with a combined heaving and pitching motion. Two operation points presenting different levels of turbulent structure generation were used. The first case with high reduced frequency of 0.18 presents smooth trailing edge flow while the case with lower reduced frequency of 0.08 exhibits important leading edge vortex shedding and more turbulent structures near wake.

It was shown that for the case with high reduced frequency, cycle-averaged and instantaneous performance parameters closely match between the Spalart-Allmaras and the Scale-Adaptive turbulence models. For the case with important LEVS, several discrepancies were observed on turbulent structures in the hydrofoil wakes. Relative differences on the efficiency between results from SAS model and S-A models remain small and seem to be caused by the differences observed on the moment coefficient peak values since the peak values of vertical force coefficient closely match.

In 3D, using SAS or S-A does not change notably the instantaneous forces on the oscillating foil. However, the SAS model leads to finer structures in the wake, which may have an important effect on an eventual downstream foil. The next step in this ongoing study is to simulate such multiple-foils interactions.

ACKNOWLEDGMENTS

Financial support from the Natural Sciences and Engineering Research Council of Canada (NSERC) and Les Fonds Québécois de la Recherche sur la Nature et les Technologies (FQRNT) is gratefully acknowledged. Computations were made on the supercomputers Colosse from Laval University and Guillimin from McGill University, managed by Calcul Québec and Compute Canada. The operation of these supercomputers is funded by the Canada Foundation for Innovation (CFI), NanoQuébec, RMGA and the Fonds de recherche du Québec - Nature et technologies (FRQ-NT).

REFERENCES

[1] McKinney, W., DeLaurier, J., The Wingmill: An Oscillating-wing Windmill, *Journal of Energy*, Vol. 5, No. 2, 1981, pp.109-115.

[2] Jones, K. D., Lindsey, K., and Platzer, M. F., An Investigation of the Fluid-Structure Interaction in an Oscillating-Wing Micro-Hydropower Generator, *Fluid Structure Interaction 2*, edited by Chakrabarti, Brebbia, Almorza, and Gonzalez-Palma, WIT Press, Southampton, England, U.K., 2003, pp. 73-82.

[3] Kinsey, T. and Dumas, G., Parametric study of an oscil-

lating airfoil in power-extraction regime. *AIAA Journal*, Vol. 46, No. 6, 2008, pp. 1318-1330.

[4] Kinsey, T., Dumas, G., Lalande, G., Ruel, J., Méhut, A., Viarouge, P., Lemay, J., Jean, Y., Prototype Testing of a Hydrokinetic Turbine Based on Oscillating Hydrofoils, *Renewable Energy J.*, Vol. 36, No. 6, 2011, pp. 1710-1718.

[5] Kinsey, T. and Dumas, G., Computational Fluid Dynamics Analysis of a Hydrokinetic Turbine Based on Oscillating Hydrofoils, *J. Fluid Eng. - Trans ASME*, Vol. 134, No. 2, 2012, pp.021104.

[6] Kinsey, T. and Dumas, G., Three-Dimensional Effects on an Oscillating-Foils Hydrokinetic Turbine, *J. Fluid Eng. - Trans ASME*, Vol. 134, No.7, 2012, pp.071105.

[7] Kinsey, T. and Dumas, G., Optimal Tandem Configuration for Oscillating-Foils Hydrokinetic Turbine, *J. Fluid Eng. - Trans ASME*, Vol. 134, No. 3, 2012, pp.031103.

[8] Betz, A.,"Das Maximum der Theoretisch Möglichen Ausnützung des Windes Durch Windmotoren", Zeitschrift für das Gesamte Turbinenwesen, Vol. 26, Sept. 1920, pp.307-309.

[9] ANSYS INC., 2012, ANSYS FLUENT 14.5 User's Guide. http://www.fluent.com.

[10] Fröhlich, J. and von Terzi, D., Hybrid LES/RANS methods for the simulation of turbulent flows, *Progress in Aerospace Sciences*, Vol. 44, Issue 5, 2008, pp.349-377.

[11] Menter, F. and Egorov, Y., 2010, The Scale-Adaptive Simulation Method for Unsteady Turbulence Flow Predictions. part1: Theory and Model Description, *J. Flow, Turbulence and Combustion*, Vol. 85, No. 1, 2012, pp. 113-138.